Analytical Approach to Recovering Bone Porosity From Effective Complex Shear Modulus

Carlos Bonifasi-Lista
Department of Bioengineering,
University of Utah,
72 South Central Campus Drive, Room 2646,
Salt Lake City, UT 84112
e-mail: cb28@utah.edu

Elena Cherkaev[1]
Department of Mathematics,
University of Utah,
155 South 1400 East, JWB 233,
Salt Lake City, UT 84112
e-mail: elena@math.utah.edu

Yener N. Yeni
Bone and Joint Center,
Henry Ford Hospital,
2799 West Grand Boulevard,
Detroit, MI 48202
e-mail: yeni@bjc.hfh.edu

This work deals with the study of the analytical relations between porosity of cancellous bone and its mechanical properties. The Stieltjes representation of the effective shear complex modulus of cancellous bone is exploited to recover porosity. The microstructural information is contained in the spectral measure in this analytical representation. The spectral function can be recovered from the effective measurements over a range of frequencies. The problem of reconstruction of the spectral measure is very ill-posed. Regularized algorithm is derived to ensure stability of the results. The proposed method does not use any specific assumptions about the microgeometry of bone. The approach does not rely on correlation analysis, it uses analytical relationships. For validation purposes, complex shear modulus over a range of frequencies was calculated by the finite element method using micro-computed tomography (micro-CT) images of human cancellous bone. The calculated values were used in numerical algorithm to recover bone porosity. At the microlevel, bone was modeled as a heterogeneous medium composed of trabeculae tissue and bone marrow treated as transversely isotropic elastic and isotropic viscoelastic materials, respectively. Recovered porosity values are in excellent agreement with true porosity found from the corresponding micro-CT images. [DOI: 10.1115/1.4000082]

1 Introduction

Mechanical behavior of a composite material depends on parameters of its microstructure such as number and volume fractions of its constituents and their relative arrangement at the microlevel. Different approaches have been developed to calculate effective material properties from microstructural information [1,2]. Bone is a hierarchical composite whose mechanical properties are scale-dependent. Its effective mechanical properties and, therefore, the ability of bone to withstand fracture depend on its structural organization. Micro-macro strategies are becoming more important for the mechanical characterization of bone [3,4]. The influence of porous structure on the elastic properties was analyzed in Ref. [5] and used to estimate partial porosities from overall elastic moduli for a particular type of morphology of cortical bone.

Bergman [6] introduced an analytical Stieltjes representation for the effective complex permittivity of a two component mixture. This representation was exploited to bound effective permittivity of composites given information (volume fraction) about its constituents [6–8]. Later, this approach was used to derive bounds for the effective elastic properties of a composite material [9,10]. This technique was recently applied in biomechanics to calculate bounds for the effective shear modulus of cancellous bone filled with bone marrow subjected to torsion within the framework of linear viscoelastic isotropic materials [11].

The Stieltjes representation analytically relates effective properties to microstructural information through the spectrum of a linear operator that naturally arises in the problem [6,8]. Using this representation, bounds for effective properties of composite material can be derived from information about its constituents (properties, volume fractions, and type of symmetry). These techniques are very successful when the constituents of the composites have a low contrast ratio. For high contrast constituents, bounds are very broad, which restrict their use. This fact has prevented the use of this technique in biomechanics where constituents usually have very different mechanical properties such as in cancellous bone considered as a composite of trabecular tissue and bone marrow. The Stieltjes representation can also be used to recover microstructural information of clinical relevance from effective properties. In this line of research, a method called inverse homogenization was developed to estimate parameters of the microstructure of the composite medium using measurements of the effective complex permittivity [12]. The method is based on the reconstruction of the spectral measure in the Stieltjes analytic representation [13,12]. The spectral measure contains all information about the microgeometry. It was shown that the spectral measure can be uniquely recovered from the measurements of the effective property over a range of frequencies [12]. However, the reconstruction requires regularization because the problem is ill-posed. After recovery of the spectral function, geometric parameters can be calculated. In particular, the zero moment of the spectral function equals to the volume fraction of one of the components; higher order moments contain further microstructural information [6,8,14]. This method was successfully applied to estimation of brine volume in sea ice from measurements of effective permittivity in Ref. [15], where comparison with laboratory measurements of the brine volume of sea ice demonstrated an excellent agreement. The advantage of the method is that no a priori information about the microstructure is needed.

Within the framework of linear viscoelasticity, the inverse homogenization method was used to successfully recover the porosity of cancellous and compact bone from measurements of its complex shear modulus. Bone microstructures were idealized as third rank laminates or as a hexagonal array of cylinders [16–18]. Idealized micro-architecture was used in these studies for valida-

tion purposes. The ill-conditioning of the problem might change drastically with real microgeometry. In the present paper, we used micro-CT images of real bone microstructures to address this problem. The developed method does not use any specific assumptions about the microgeometry of the composite and is applicable to any two-phase composite medium. In the absence of experimental measurements of the effective shear modulus, we used finite element method numerical simulations to calculate complex shear modulus of cancellous bone for different frequencies. In any case, experimental validation is very expensive and time consuming, and computer simulations performed at the first stage of validation can save time and money. Besides the data of the complex shear modulus of cancellous bone, the method requires a priori knowledge of the properties of the constituents (trabeculae tissue and bone marrow), which in practice could be known with some uncertainty. These properties are subject-specific and depend also on pathologic conditions. To address this issue, normally distributed random functions were added as noise to simulate uncertainty in the properties of the constituents. A different normally distributed random function was added to the effective complex modulus to simulate possible experimental errors. We used these data as input for the developed method and reconstructed the spectral function by solving inverse problem. Then the bone porosity was calculated as a zero moment of the spectral function. Results of numerical simulations show that the values of porosity calculated from the effective shear modulus are in good agreement with the model values even for data with high level of uncertainty.

The outline of the paper is as follows: first, in Sec. 2, we very briefly introduce the Stieltjes representation for the effective complex shear modulus of a heterogeneous material. Next, we develop the forward model, which is used to determine the effective properties of cancellous bone from properties of its constituents: trabecular tissue and bone marrow. In Sec. 4, we present the inverse algorithm used to recover porosity from given effective properties. Section 5 contains the results of numerical simulations and discussion.

2 Spectral Representation of Effective Material Properties

A Stieltjes function with special analytical properties representing the effective complex permittivity ϵ^* of a two component mixture was introduced to derive bounds for the effective complex permittivity of a binary composite material [6–8]. The Stieltjes analytical representation was also used to extract specific information about the microstructure [19,20,15,21,13,12,22]. This representation of the effective permittivity of the composite depends explicitly on the properties of its constituents ϵ_1 and ϵ_2 through a complex variable s defined in terms of the permittivity of the materials in the mixture. For a binary composite, the representation for a function $F(s)=1-\epsilon^*/\epsilon_2$ is [6,14]

$$F(s) = 1 - \frac{\epsilon^*}{\epsilon_2} = \int_0^1 \frac{d\eta(t)}{s-t}, \quad \text{where} \quad s = \frac{1}{1-\epsilon_1/\epsilon_2} \quad (1)$$

Here ϵ^* is the effective complex permittivity of the mixture and ϵ_i is the permittivity of the ith material, $i=1,2$. This representation is valid for other physical properties such as diffusivity and electrical or thermal conductivity. The nth moment η_n of the function η is

$$\eta_n = \int_0^1 t^n d\eta(t) \quad (2)$$

It was proved [6,8] that the zero moment of the measure η gives the volume fraction of one of the components. Higher order moments give further microstructural information [14,23].

In Refs. [9,10], this Stieltjes representation was generalized for the case of elastic properties. However, due to the higher order of

tensors involved in continuum mechanics, the relation between the variable s in Eq. (1) and the properties of the constituents is more complicated. An exception is the case of torsion where the problem can be reduced to the form similar to the problem for complex permittivity. Under simple assumptions on torsion behavior of the composite, Tokarzewski et al. [11] showed that for linear viscoelastic constituents, the effective complex shear modulus has the Stieltjes representation of $F(s)$ of the form of Eq. (1) with s retaining its connection with the properties of the constituents. The proof involves two-scale asymptotic expansions of the displacement vector and is done under the supposition that the composite follows Saint-Venant assumptions for torsion. This Stieltjes representation for complex shear modulus is valid as long as the constituents in the microstructure are isotropic or/and transversely isotropic, and it is independent of the relative arrangement of the constituents. In other words, the composite at the macrolevel can have any symmetry or none at all [18]. The method is valid for two-dimensional (2D) sections of composite and also for three-dimensional (3D) volumes as long as the Saint-Venant principle for torsion holds [11,18]. In this case, the Stieltjes representation is given exactly by Eq. (1), we recast it here in terms of shear moduli

$$F(s) = 1 - \frac{\mu_{\text{eff}}^*}{\mu_2} = \int_0^1 \frac{d\eta(t)}{s-t}, \quad \text{where} \quad s = \frac{1}{1-\mu_1/\mu_2} \quad (3)$$

Here μ_{eff}^* is the effective complex shear modulus of the composite, and μ_i is the complex shear modulus of material i, $i=1,2$. In this case, the zero moment of the function η gives us the volume fraction of one of the constituents

$$\eta_0 = \int_0^1 d\eta(t) = p_1 \quad (4)$$

Here, p_1 is the volume fraction of the constituent with shear modulus μ_1. In our case it might be either the volume fraction of bone marrow or of trabecular tissue depending on how the problem is formulated.

Summarizing, the spectral representation in Eq. (3) separates information about the properties of the constituents contained in variable s from geometric information about the bone morphology. This geometric information is enclosed in the spectral function $\eta(t)$. This representation can be generalized to multimaterial composites and used to bound their effective properties.

3 Effective Complex Shear Modulus of Bone: Forward Model

In order to recover porosity using the spectral function $\eta(t)$, experimental (in-vivo or in-vitro) values of effective complex shear μ^* of cancellous bone and its constituents in a range of frequencies are required. Five micro-CT scans of a T12 vertebra of a 79 year old white male donor were used in this work. One of the micro-CT images is shown in Fig. 1. In the absence of experimental data, the effective complex shear modulus of the bone samples was numerically calculated using the finite element method. At the microlevel, we consider cancellous bone as a composite of trabecular tissue and bone marrow. Trabecular tissue is considered to be transversely isotropic, and bone marrow is modeled as an isotropic fluidlike solid. Under the assumption that cancellous bone satisfies the Saint-Venant principle for infinitesimal torsion, the governing equation at the microlevel can be reduced to [18]

$$\nabla \cdot \mu(\mathbf{x}) \nabla U(\mathbf{x}) = 0 \quad \text{in} \quad \Omega \quad (5)$$

Here $U(\mathbf{x})$ is a potential function such that $\nabla U(\mathbf{x})$ is the shear strain ϵ, and $\mu(\mathbf{x})$ is the complex shear modulus of the composite. Having introduced a characteristic function $\chi(\mathbf{x})$ that takes a value of 1 if $\mathbf{x}$ is in the bone marrow phase, $\mathbf{x} \in \Omega_1$, and 0 if $\mathbf{x}$ is in
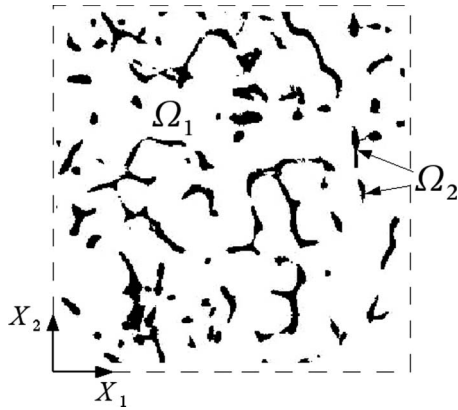
Fig. 1 Example of a micro-CT scan of a T12 vertebra used in the numerical simulations. The subdomain Ω_1 is filled with bone marrow, and Ω_2 is filled with trabecular tissue.
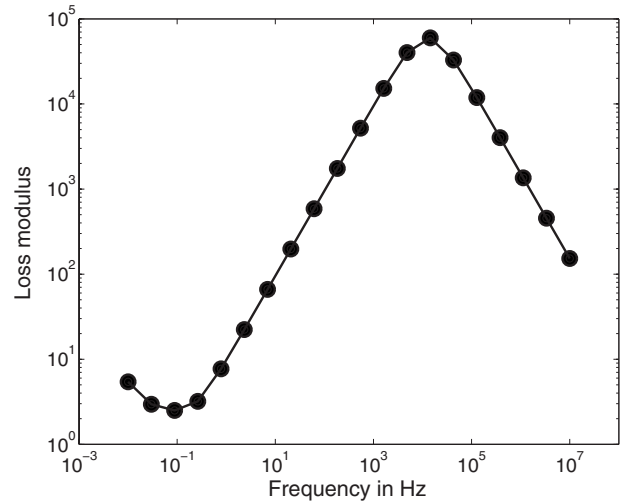

Fig. 2 Loss modulus of the effective complex shear corresponding to hexagonal structure composed of cylinders filled with trabecular tissue and matrix representing bone marrow. Results calculated by finite element method of solution of Eq. (5) are given by circles (●), and the solid line (−) represents the analytical solution derived in Ref. [11].

trabecular tissue, $\mathbf{x} \in \Omega_2$, we can represent shear function $\mu(\mathbf{x})$ as $\mu(\mathbf{x}) = \chi(\mathbf{x})\mu_1 + (1 - \chi(\mathbf{x}))\mu_2$. Here, μ_1 and μ_2 are the complex shear moduli of bone marrow and trabecular tissue, respectively. Notice, that μ_i is a complex function that depends on frequency.

The boundary conditions for partial differential equation (5) are given by a drop of potential U along the X_1 axis and periodic no flux conditions on the upper and lower edges of the domain $\Omega = \Omega_1 \cup \Omega_2$ (see Fig. 1).

The reduced governing Eq. (5) has the advantage that the entire material property tensors are not needed, only the shear moduli of bone marrow and trabecular tissue are required to calculate the distribution of shear strains and stresses in the sample. Proof of the validity of the reduced governing equation can be found in Refs. [11,18]. Equation (5) was solved by the finite element method implemented in COMSOL MULTIPHYSICS for real bone microstructures retrieved from the micro-CT scans.

The effective shear modulus of cancellous bone can be calculated from the distribution of numerically determined stresses and strains through the following relation:

$$\langle \sigma \rangle = \mu^* \langle \epsilon \rangle \tag{6}$$

Here, σ and ϵ are the shear stress and strain, and the sign $\langle \cdot \rangle$ represents the averaging operation such that

$$\langle \sigma \rangle = \frac{1}{V} \int_{\Omega} \sigma dV \tag{7}$$

with V being the volume of the computational domain Ω.

For validation purposes, we compared the finite element implementation with the analytical solution for hexagonal cylindrical arrays derived in Refs. [11,18]. In this validation study, the cylinders were filled with trabecular tissue and the matrix material represented bone marrow. The results are in perfect agreement, they are shown in Fig. 2. The effective shear modulus of the hexagonal structure calculated using the finite element method is shown by black circles, while the semi-analytical solution calculated using the method of Tokarzewski et al. [11] is given by the solid line. The excellent agreement of the numerical results obtained with two different methods justifies the use of the finite element method in calculations of the shear modulus for the real bone morphology.

3.1 The Shear Properties of Trabecular Tissue and Bone Marrow. Multidirectional properties in compression of human trabecular tissue were recently determined with subnanometer resolution [24]. Results suggest that trabecular or cancellous tissue at the microlevel can be represented as a transversely isotropic material. Poisson ratios and elastic moduli in the longitudinal, postero-anterior and latero-medial directions of twenty one speci-

mens of cancellous bone tissue of seven fresh femoral heads were reported in Ref. [24]. Using the constitutive theory of linear elasticity we determined the shear modulus from the reported data. For a transversely isotropic material with x_3 taken as the axis of symmetry, shear modulus μ_{12} of trabecular is given by $\mu_{12} = E_{12}/(1 + \nu_{12})$ with $\sigma_{12} = \mu_{12}\epsilon_{12}$. Here, E represents the Young's modulus, and ν is the Poisson ratio. Therefore, using data from Ref. [24], the shear modulus of trabecular tissue is calculated as $\mu_{12} = \mu = 2.23$ GPa. This value was used in numerical simulations with the finite element model. It is known that bone marrow is a thixotropic material, but we do not model the thixotropic properties because we are interested in the steady state response of bone marrow and not in the transient response between states for different strain rates. The fluid phase behaves as a Newtonian fluid [25]. In shear, bone marrow presents a non-Newtonian behavior due to the solid phase. However, this non-Newtonian behavior can be modeled as piecewise linear, and it can be considered as linear within a certain range of strain rate [26]. The solid part of bone marrow is composed of cells whose viscoelastic properties can be described by a standard linear solid model [27]. Unfortunately, there are not enough experimental data to fully characterize the non-Newtonian behavior of bone marrow. The model of bone marrow we present here is derived from the non-Newtonian shear rate dependent viscoelastic properties published in Ref. [26]. The proposed model follows ideas similar to the one used in Ref. [28] for modeling the non-Newtonian behavior of blood.

We model the shear response of bone marrow using a four-parameter Maxwell model, which is composed of two parallel Maxwell elements (see Fig. 3); it behaves as viscoelastic fluid. Its viscoelastic relaxation function depending on time $t, t \geq 0$ consists of two decaying exponentials characterizing the fading memory

$$G(t) = \sum_{i=1}^{2} G_i e^{-t/\tau_i} \tag{8}$$

Here G_i is the elastic spring constant of the ith Maxwell element, τ_i is its relaxation time, and $\tau_i = \eta_i / G_i$ with η_i representing the viscosity or viscous resistance coefficient of the ith dashpot. The corresponding complex shear modulus is given by

$$\mu_1(\omega) = \sum_{i=1}^{2} \left(\frac{G_i \omega^2 \tau_i^2}{1 + \omega^2 \tau_i^2} + j \frac{G_i \omega \tau_i}{1 + \omega^2 \tau_i^2} \right) \tag{9}$$
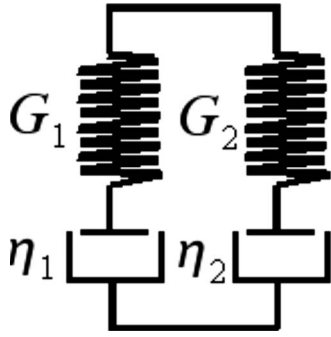
Fig. 3 Standard four-parameter Maxwell model

where ω is the frequency in rad/s.

To characterize the non-Newtonian behavior of bone marrow due to its solid part, we assume that η_i depends on strain rate $\dot{\epsilon}$

$$\eta_i = \eta_{0,i} T_i(\dot{\epsilon}), \quad i = 1,2 \tag{10}$$

$T(\dot{\epsilon})$ is a degradation function that characterizes the non-Newtonian behavior of bone marrow, and $\eta_{0,i}$ is the viscosity at the ground state of equilibrium corresponding to the Maxwell element i. Properties in the ground state of equilibrium can be measured by the application of very small forces and deformations that do not disrupt the internal structure [28]. Sobotková et al. [26] reported the steady flow viscosity $\eta_s(\dot{\epsilon})$ for human bone marrow (solid+fluid parts). The relation between the steady flow viscosity and the ground state viscosity is given by

$$\eta_0 = \lim_{\dot{\epsilon} \to 0} \eta_s(\dot{\epsilon}) \tag{11}$$

To model the steady state flow viscosity of bone marrow, we approximated data reported in Ref. [26] using nonlinear regression. Our model for steady flow viscosity is the following:

$$\eta_s(\dot{\epsilon}) = \sum_{i=1}^{2} P_i(\dot{\epsilon}) \quad \text{where} \quad P_i(\dot{\epsilon}) = a_i + \frac{b_i}{(1 + e^{\tau_i(\dot{\epsilon} - \epsilon_{i,0})})^c}, \quad i = 1,2 \tag{12}$$

with a_i, b_i, and $\epsilon_{i,0}$ being constants and $\dot{\epsilon}$ being the strain rate. The results of the nonlinear regression analysis are given in Fig. 4. The
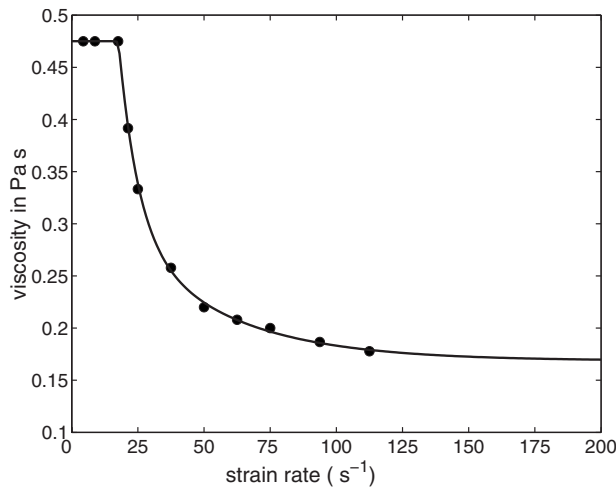
values for the parameters are presented in Table 1. From Eqs. (11) and (12), we obtain the ground state viscosity as

$$\eta_0 = \sum_{i=1}^{2} \eta_{0,i} = \sum_{i=1}^{2} a_i + \frac{b_i}{(1 + e^{-\tau_i \dot{\epsilon}_{i,0}})^c} \tag{13}$$

In the absence of experimental data that would determine the degradation functions $T_i(\dot{\epsilon})$ in Eq. (10), we assume $T_i(\dot{\epsilon}) = P_i(\dot{\epsilon})$ as an approximation. This has the advantage that the complex shear modulus of bone marrow is very insensitive to changes of strain rate between 10^{-5} s^{-1} and 10 s^{-1}. This is the range where bone marrow behaves as a Newtonian fluid (Fig. 4), and this insensitivity allows to approximate the strain rate dependent η_i of our model (Fig. 3) given in Eq. (10) using a fixed strain rate $\dot{\epsilon}$ no greater than 20 s^{-1} (linear regime). In our simulations we set it to 10 s^{-1}. In this way, for a sufficiently small range of frequencies in harmonic motion, we can ensure that the maximum shear rate will be less than 20 s^{-1} and therefore within the linear response of bone marrow. Experimentally this can be achieved by reducing the amplitude of the harmonic motion as the frequency increases.

We assume that the elastic coefficients of the model are not strain rate dependent. The elastic constants are approximated using properties of fat tissue in breast. The instantaneous shear modulus G_g of adipose tissue from breast was reported to be around 0.5–25 kPa [29]. For the discussed Maxwell model, the instantaneous modulus is given by

$$G_g = G_1 + G_2 \tag{14}$$

To regard this condition, we assigned values for G_i in the model such that their sum is equal to 25 kPa.

Having all the parameters for the model of bone marrow, we calculate the shear complex modulus using Eq. (9). Figure 5 shows the real and imaginary parts (storage and loss moduli, respectively) of the complex shear modulus of bone marrow. Figure 6 shows the effective complex shear modulus of cancellous bone calculated for one of the specimens.

The calculated values of the effective properties are quite low,

Fig. 4 Steady flow viscosity: filled circles ● show values derived from flow curve of human marrow (40 years old man) at 37 °C [26]; continuous solid line shows approximation obtained by nonlinear regression using Eq. (12). Correlation factor r^2 =0.99. Parameters for our model are listed in Table 1.
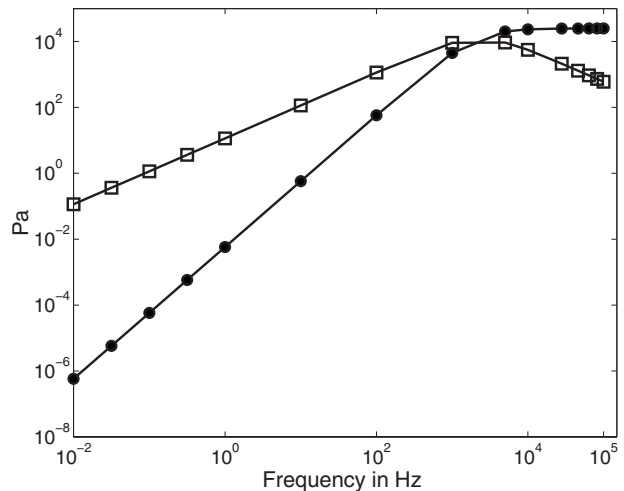

Fig. 5 Complex shear modulus for bone marrow: filled dots ● show storage modulus, and squares □ indicate loss modulus
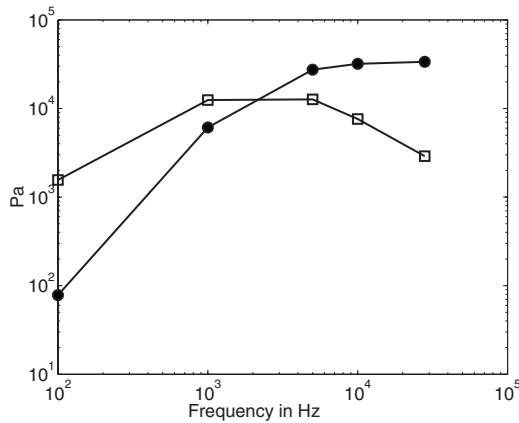
Fig. 6 Effective complex shear modulus of cancellous bone (bone marrow+trabecular tissue) determined computationally using the finite element method. Values at only four frequencies were computed and used in further calculations. Filled dots ● show storage modulus, and squares □ indicate loss modulus.

but this could be explained by specifics of the two-dimensional problem and the neglected connectivity of trabecular tissue. As it was mentioned previously, due to our assumptions, the problem at the microstructural level is reduced to solution of a partial differential equation for a potential function. In the computational domain, the trabecular tissue is completely surrounded by bone marrow, and therefore the boundary conditions are directly applied to bone marrow. Due to the high viscosity of bone marrow, most of the energy is dissipated before being transmitted to the trabecular tissue. However, our computational model is sufficient to address the problem of effect of geometry in the spectral representation of effective complex shear modulus in terms of ill-conditioning of the inverse problem.

4 Recovering Porosity: The Regularized Inverse Problem

This section discusses the problem of recovering porosity and the spectral function $\eta(t)$ from measurements of the function $F(s)$ given in Eq. (3). It is shown in [12] that the spectral function η in this integral representation can be uniquely reconstructed if the effective property of the composite is known along some arc in the complex plane s. Such data can be obtained from measurements in an interval of frequency provided that at least one of the constituents is frequency dependent [12]. This method was used successfully to recover porosity of bone from effective shear modulus for idealized bone microstructure [16,18].

Function $\eta(t)$ can be reconstructed either from the real or imaginary part of function $F(s)$ using Eq. (3). Using $s=x+iy$ and separating real and imaginary parts of function $F(s)$, we obtain

$$\mathrm{Re}(F(s)) = \int_0^1 \frac{(x-t)d\eta(t)}{(x-t)^2+y^2}, \quad \mathrm{Im}(F(s)) = -\int_0^1 \frac{yd\eta(t)}{(x-t)^2+y^2} \tag{15}$$

To find function $\eta(t)$, one needs to solve one of these integral equations. However, the reconstruction problem is ill-posed. This means that small variations in the data or computational noise can lead to arbitrary large variations in the solution. The high contrast between the properties of trabecular and bone marrow tissues tremendously increases ill-posedness of the problem, making the values of the complex variable s corresponding to measurements at different frequencies to be very close to each other on the complex plane. In this case, previously developed regularization techniques do not work very efficiently. To deal with this problem,

a change in variable $t=e^z$ is introduced. In terms of this new variable z, integrals above can be rewritten as follows. The integral equation for the real part of the function $F(s)$ is transformed to

$$\mathrm{Re}(F(s)) = \int_{-\infty}^0 \frac{(x-e^z)\varphi(e^z)}{(x-e^z)^2+y^2}e^z dz \tag{16}$$

and for the imaginary part:

$$\mathrm{Im}(F(s)) = -\int_{-\infty}^0 \frac{y\varphi(e^z)}{(x-e^z)^2+y^2}e^z dz \tag{17}$$

Here, we have written $d\eta(t)$ as $d\eta(t)=\varphi(t)dt$.

Assume that the values of effective complex modulus μ^* are known at several frequencies, $\omega_1, \omega_2, \ldots, \omega_m$. These data provide discrete values of the function $F(s):F(s_1),\ldots,F(s_m)$. We discretize the integrals in Eqs. (16) and (17), let K be such discretization of integral corresponding to either real part or imaginary part of $F(s)$ in Eqs. (16) and (17). Let vector f be the corresponding either real or imaginary part of $F(s_k)$, $k=1,\ldots,m$, and vector g contain the discretized values of function $\varphi(e^z)$. Solution of integral equations given by Eq. (16) or Eq. (17) can be formulated as a least-squares minimization problem. To ensure a stable solution of the ill-posed problem we introduce a stabilization functional and formulate a regularized least-squares minimization problem

$$\min_{g\in R^n}\{\|Kg-f\|_2^2 + \alpha\|g\|_2^2\} \tag{18}$$

Here $\|\cdot\|_2$ represents the Euclidean norm, and α is a regularization parameter. Solution of minimization problem (18) is provided by the Euler equation [30]

$$g_\alpha = (K^TK+\alpha I)^{-1}K^Tf \tag{19}$$

where K^T is the transpose of K and can be expressed in terms of the singular value decomposition (SVD) of the matrix K. Singular value decomposition of K is given as

$$K_{m\times n} = U_{m\times m}\Sigma_{m\times n}V_{n\times n}^T$$

where the matrix Σ has nonzero entries s_i on the diagonal; these values s_i are the singular values of K. The left singular vectors u_i are the column vectors of matrix U, and the right singular vectors v_i are the column vectors of matrix V. Using the pseudoinverse K^+ of K, $K^+=V\Sigma^+U^T$, where Σ^+ is the transpose of Σ in which s_i is replaced by s_i^{-1}, the solution g_α can be expressed in the form

$$g_\alpha = \sum_{i=1}^m \frac{s_i(u_i^Tf)}{s_i^2+\alpha}v_i \tag{20}$$

The regularization parameter α determines the weight of each singular value of K in the reconstruction of the vector g. Parameter α must be chosen appropriately so that the solution is close to the true solution. The L-curve method [30] was used to choose the proper regularization parameter α. This method consists in plotting the log of the squared norm of the regularized solution, $\log(\|g\|_2^2)$ against the log of the squared norm of the regularized residual $\log(\|Kg-f\|_2^2)$ for a range of values of the regularization parameter. This curve typically has an L shape, and the proper value of the parameter α corresponds to the corner of this curve. To find the corner point and the corresponding value of α, we use method of Hansen and O'Leary [31] who recommended picking the point of maximum curvature. Once the approximation g to the function φ is reconstructed, the porosity can be recovered using Eq. (4) rewritten in terms of $\varphi(z)$

$$p_1 = \int_{-\infty}^0 \varphi(z)e^z dz \tag{21}$$

Table 2 Porosity recovered from real part of $F(s)$. No noise is added.

P_{true}	P_{calc}
0.9260	0.9422
0.9257	0.9177–0.9258–0.9333
0.9338	0.9539
0.9244	0.9527
0.8987	0.8984–0.9086

5 Results and Discussion

The minimization technique described above allows us to recover the spectral function φ and therefore the porosity of cancellous bone given the effective properties of bone and of its constituents, trabecular tissue and bone marrow, in a range of frequencies. The forward model presented in Sec. 3 was used to numerically simulate effective shear modulus μ^* of cancellous bone for each of the five specimens at five different frequencies in a range of frequencies from 10^2 Hz to 3×10^4 Hz. The shear modulus of bone marrow was taken as μ_1, and μ_2 was assigned as the complex modulus of trabecular tissue. These data were used in the developed algorithm to calculate estimates for the bone porosity. Results of reconstruction of porosity from real part of $F(s)$ for all five specimens are shown in Table 2, where P_{true} corresponds to the true porosity of the specimens, and P_{calc} stands for the recovered value. No noise was added to the input data in this case, only computational noise was present.

In some cases, the L-curve algorithm that we used to determine the appropriate value of the regularization parameter α suggests several possible values, more specifically, the corresponding curvature curve, as the curvature graph shown in Fig. 7, has several local maxima. Most of them give values of porosity outside the unit interval, and hence they were automatically disregarded. Within the feasible range of porosities, only one maximum happens for most cases. In few cases, there were two or even three maxima whose corresponding porosities were taken as the lower and upper bounds for the true porosity. This is reflected in the results shown in Table 2, as well as in other calculated values shown further.

The next series of numerical simulations was done to test the robustness of the developed minimization technique. Effective properties (macroscale) can be determined experimentally in-vitro and estimated in-vivo within some error. Properties of bone marrow and trabecular tissue (microscale) cannot be measured in-
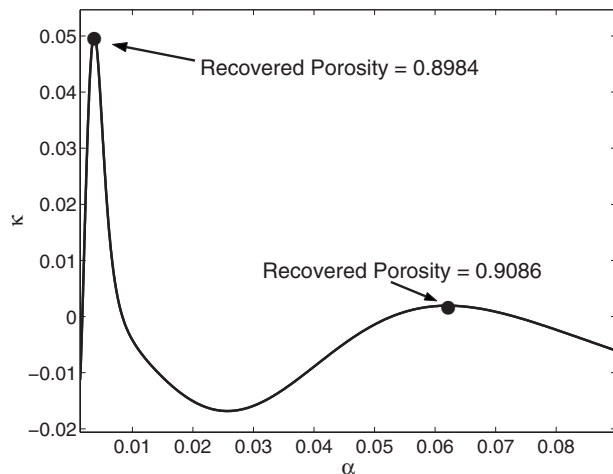

Fig. 7 Curvature κ versus regularization parameter α. Two local maxima are shown together with the corresponding recovered porosities. True porosity = 0.8987.

Table 3 Calculated estimates P_{calc} of bone porosity for specimen with true porosity 0.9260. Characteristics of noise added to the material properties are reflected in noise$_\mu$ columns as (mean±standard deviation).

P_{true}	P_{calc}	noise$_{\mu_1}$	noise$_{\mu_2}$	noise$_{\mu^*}$
0.9260	0.9545	3.31 ± 2.33	3.72 ± 2.91	1.96 ± 1.33
0.9260	0.9629	8.24 ± 6.14	7.99 ± 7.23	18.94 ± 16.57
0.9260	0.9612	13.27 ± 9.32	11.89 ± 9.31	2.61 ± 1.47
0.9260	0.9437	10.35 ± 6.86	11.31 ± 9.08	9.34 ± 5.63
0.9260	0.9612	20.60 ± 15.34	15.99 ± 14.47	6.35 ± 5.52
0.9260	0.9588	30.07 ± 22.48	27.18 ± 22.43	5.70 ± 6.62
0.9260	0.9122	27.81 ± 24.68	37.16 ± 23.99	27.15 ± 20.69
0.9260	0.9470	41.39 ± 22.45	31.49 ± 18.88	8.53 ± 4.97
0.9260	0.9328	41.39 ± 28.02	45.07 ± 37.30	5.04 ± 5.88
0.9260	0.9566	43.19 ± 31.33	27.36 ± 17.79	18.19 ± 12.17
0.9260	0.9405	51.60 ± 42.60	42.16 ± 31.14	37.91 ± 26.95
0.9260	0.9450	48.80 ± 29.85	52.22 ± 36.51	50.56 ± 22.13

vivo, and even though they can be tabulated from in-vitro experiments, these tabulated values can differ from the true values because they depend on physiological conditions and are subject-dependent. To simulate this situation, different normally distributed random functions were added as "noise" to the material properties of bone marrow and trabecular tissue. Noise was also added to the effective complex shear modulus μ^* determined using the finite element method for the five samples to imitate possible experimental errors.

For three different specimens, Tables 3–5 show the recon-

Table 4 Calculated estimates P_{calc} of bone porosity for specimen with true porosity of 0.9257. Characteristics of noise added to the material properties are reflected in noise$_\mu$ columns as (mean±standard deviation).

P_{true}	P_{calc}	noise$_{\mu_1}$	noise$_{\mu_2}$	noise$_{\mu^*}$
0.9257	0.9196–0.9354	2.62 ± 2.40	2.14 ± 1.38	2.50 ± 1.55
0.9257	0.9402	9.27 ± 5.58	9.77 ± 6.94	7.85 ± 4.69
0.9257	0.9463	29.03 ± 18.68	17.78 ± 15.56	11.17 ± 7.14
0.9257	0.9348–0.9598	22.34 ± 21.87	20.59 ± 25.24	12.12 ± 11.11
0.9257	0.9649	60.97 ± 29.90	15.96 ± 14.84	29.45 ± 27.97
0.9257	0.9508	10.35 ± 8.29	22.55 ± 14.10	28.72 ± 15.63
0.9257	0.9303	31.17 ± 26.44	35.45 ± 35.59	21.94 ± 25.58
0.9257	0.9257	48.13 ± 21.62	28.12 ± 18.24	54.11 ± 27.28
0.9257	0.9325	40.23 ± 35.84	42.02 ± 45.79	32.62 ± 18.79
0.9257	0.9304	60.40 ± 43.68	79.05 ± 40.21	14.86 ± 8.99

Table 5 Calculated estimates P_{calc} of bone porosity for specimen with true porosity 0.8987. Characteristics of noise added to the material properties are reflected in noise$_\mu$ columns as (mean±standard deviation).

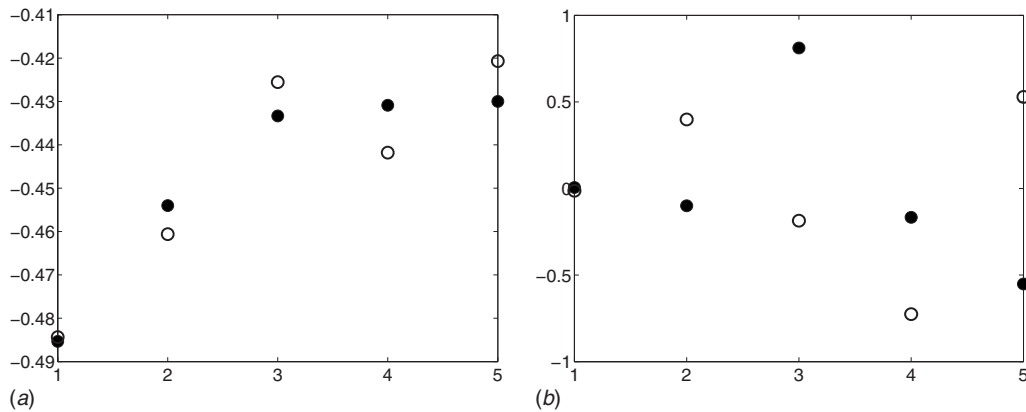| P_{true}	P_{calc}	noise$_{\mu_1}$	noise$_{\mu_2}$	noise$_{\mu^*}$
0.8987	0.8849	7.31 ± 6.52	7.64 ± 8.32	9.32 ± 5.37
0.8987	0.8978–0.9246	11.72 ± 4.85	15.41 ± 7.95	13.25 ± 7.38
0.8987	0.9113	18.57 ± 18.69	14.86 ± 12.66	17.84 ± 7.87
0.8987	0.9337	35.23 ± 25.48	46.11 ± 23.45	14.86 ± 8.99
0.8987	0.8812	42.85 ± 32.92	27.91 ± 22.89	30.97 ± 29.75
0.8987	0.8959	34.65 ± 13.80	47.44 ± 23.96	32.56 ± 30.75
0.8987	0.9385	60.56 ± 18.00	35.26 ± 22.04	36.07 ± 36.81
0.8987	0.9205	41.95 ± 12.84	46.25 ± 31.29	23.66 ± 17.45
0.8987	0.8529	48.19 ± 25.56	44.00 ± 26.29	38.99 ± 34.44
0.8987	0.9298	46.88 ± 58.62	63.35 ± 37.49	27.23 ± 23.97
0.8987	0.9219	55.08 ± 32.15	70.70 ± 47.04	29.56 ± 21.94

Fig. 8 Eigenvectors u_i for $i=1,4$. Filled dots ● show eigenvectors calculated without noise, and open circles ○ show eigenvectors calculated with noise added. Noise levels: noise$_{\mu_1}$=27.35±11.32, noise$_{\mu_2}$=30.82±15.91, and noise$_{\mu^*}$=26.49±14.77. (*a*) Eigenvector corresponding to the first eigenvalue. (*b*) Eigenvector corresponding to the fourth eigenvalue.

structed porosity when uncertainty in material properties of trabecular tissue and bone marrow were introduced as noise and noise was added to the effective shear modulus. Estimates of bone porosity were computed from the real part of $F(s)$ using information at five different frequencies in the same range of frequency: $10^2-3\times10^4$ Hz. The true porosity is shown in the column with heading P_{true}, calculated estimates are shown under P_{calc}. Characteristics of added noise are reported in columns noise$_\mu$ for $\mu=\mu_1,\mu_2,\mu^*$ as mean and standard deviation over the range of frequency for each specimen. Solutions reconstructed using regularization technique depend on the regularization parameter α. The reconstruction results show that even with high percent of error in the values of the properties of the constituents and effective modulus, the algorithm was able to recover good approximations of the true bone porosity.

Numerical experiments show that the algorithm is very stable even in the presence of large errors in the estimates of the properties of the constituents and the effective property. This phenomenon can be explained by the presence of the regularization filter. Indeed, the space of data is spanned by the eigenvectors u_i of the matrix K. However, the noise is mostly projected onto the last eigenvectors. As the error level increases, the regularization parameter α increases as well, which results in filtering out components of the solution projected on the eigenvectors corresponding to the smaller eigenvalues due to the factor $s_i/(s_i^2+\alpha)$ in Eq. (20). The noise is filtered out together with these eigenvectors. The dominant eigenvalues and eigenvectors are practically unaltered when noise is added, hence, the information stored in the first eigenvectors is recovered with almost no loss. The information contained in the dominant eigenvectors (usually the first and/or second one) is enough to recover porosity successfully. This can be seen in Fig. 8 where after adding high levels of error (noise) to the measurements on one of the specimens, the first eigenvector is not affected as much as the fourth eigenvector. In this case, the porosity recovered from noisy data is 0.9279 whereas the true porosity is 0.8987.

6 Conclusions

The paper presents a method for the calculation of porosity of cancellous bone given the bone complex shear modulus and properties of bone marrow and trabecular tissue. The method is based on the spectral representation of the effective complex shear modulus of composite and reconstruction of the spectral function in this representation; this function has information about the microstructure. We also introduced a forward model for cancellous bone (trabecular tissue and bone marrow), this was done to numerically determine effective complex shear properties of bone

for different real microgeometries needed to validate the method. Micro-CT images of cancellous bone were used in computations of the bone effective properties. Numerical experiments show that the algorithm is stable even in the presence of large errors in the estimates of the properties of the constituents and the effective complex shear modulus. The advantage of this approach is that no a priori model of cancellous bone microgeometry is required.

References

[1] Kouznetsova, V., Brekelmans, W. A. M., and Baaijens, F. P. T., 2001, "An Approach to Micro-Macro Modeling of Heterogeneous Materials," Comput. Mech., **27**(1), pp. 37–48.
[2] Zaoui, A., 2002, "Continuum Micromechanics: Survey," J. Eng. Mech., **128**(8), pp. 808–816.
[3] Hollister, S. J., Fyhrie, D. P., Jepsen, K. J., and Goldstein, S. A., 1991, "Application of Homogenization Theory to the Study of Trabecular Bone Mechanics," J. Biomech., **24**(9), pp. 825–839.
[4] Hollister, S. J., Brennan, J. M., and Kikuchi, N., 1994, "A Homogenization Sampling Procedure for Calculating Trabecular Bone Effective Stiffness and Tissue Level Stress," J. Biomech., **27**(4), pp. 433–444.
[5] Sevostianov, I., and Kachanov, M., 2000, "Impact of the Porous Microstructure on the Overall Elastic Properties of the Osteonal Cortical Bone," J. Biomech., **33**(7), pp. 881–888.
[6] Bergman, D. J., 1978, "The Dielectric Constant of a Composite Material—A Problem in Classical Physics," Phys. Rep. C, **43**(9), pp. 377–407.
[7] Milton, G. W., 1981, "Bounds on the Complex Permittivity of a Two-Component Composite Material," J. Appl. Phys., **52**(8), pp. 5286–5293.
[8] Golden, K., and Papanicolaou, G., 1983, "Bounds for Effective Parameters of Heterogeneous Media by Analytic Continuation," Commun. Math. Phys., **90**(4), pp. 473–491.
[9] Kantor, Y., and Bergman, D. J., 1982, "Elastostatic Resonances—A New Approach to the Calculation of the Effective Elastic Constants of Composites," J. Mech. Phys. Solids, **30**(5), pp. 355–376.
[10] Kantor, Y., and Bergman, D. J., 1984, "Improved Rigorous Bounds on the Effective Elastic Moduli of a Composite Material," J. Mech. Phys. Solids, **32**(1), pp. 41–62.
[11] Tokarzewski, S., Telega, J. J., and Galka, A., 2001, "Torsional Rigidities of Cancellous Bone Filled With Marrow: The Application of Multipoint Pade Approximants," Eng. Trans., **49**(2–3), pp. 135–153.
[12] Cherkaev, E., 2001, "Inverse Homogenization for Evaluation of Effective Properties of a Mixture," Inverse Probl., **17**(4), pp. 1203–1218.
[13] Day, A. R., and Thorpe, M. F., 1999, "The Spectral Function of Composite: The Inverse Problem," J. Phys.: Condens. Matter, **11**, pp. 2551–2568.
[14] Bergman, D. J., 1993, "Hierarchies of Stieltjes Functions and Their Applications to the Calculation of Bounds for the Dielectric Constant of a Two-Component Composite Medium," SIAM J. Appl. Math., **53**(4), pp. 915–930.
[15] Cherkaeva, E., and Golden, K. M., 1998, "Inverse Bounds for Microstructural Parameters of a Composite Media Derived From Complex Permittivity Mea-

surements," Waves Random Media, **8**(4), pp. 437–450.

[16] Bonifasi-Lista, C., and Cherkaev, E., 2007, "Identification of Bone Microstructure From Effective Complex Modulus," *Springer Proceedings in Physics, Vibration Problems ICOVP 2005*, E. Ínan and A. Kiriş, eds., Springer, Netherlands, Vol. 111, pp. 91–96.

[17] Bonifasi-Lista, C., and Cherkaev, E., 2006, "Analytical Relations Between Effective Material Properties and Microporosity: Application to Bone Mechanics," *III European Conference on Computational Mechanics: Solids, Structures and Coupled Problems in Engineering: Book of Abstracts*, C. A. Mota Soares, J. A. C. Martins, H. C. Rodrigues, J. A. C. Ambrosio, C. A. B. Pina, C. M. Mota Soares, E. B. R. Pereira, and J. Folgado, eds., Springer, Lisbon, Portugal.

[18] Bonifasi-Lista, C., and Cherkaev, E., 2008, "Analytical Relations Between Effective Material Properties and Microporosity: Application to Bone Mechanics," Int. J. Eng. Sci., **46**(12), pp. 1239–1252.

[19] McPhedran, R. C., McKenzie, D. R., and Milton, G. W., 1982, "Extraction of Structural Information From Measured Transport Properties of Composites," Appl. Phys. A: Mater. Sci. Process., **29**(1), pp. 19–27.

[20] McPhedran, R. C., and Milton, G. W., 1990, "Inverse Transport Problems for Composite Media," Mater. Res. Soc. Symp. Proc., **195**, pp. 257–274.

[21] Tripp, A. C., Cherkaeva, E., and Hulen, J., 1998, "Bounds on the Complex Conductivity of Geophysical Mixtures," Geophys. Prospect., **46**(6), pp. 589–601.

[22] Zhang, D., and Cherkaev, E., 2008, "Pade Approximations for Identification of Air Bubble Volume From Temperature or Frequency Dependent Permittivity of a Two-Component Mixture," Inverse Probl. Sci. Eng., **16**(4), pp. 425–445.

[23] Cherkaev, E., and Ou, M.-J., 2008, "De-Homogenization: Reconstruction of Moments of the Spectral Measure of Composite," Inverse Probl., **24**, p. 065008.

[24] Park, Y. H., Cha, H. S., and Hong, J., 2007, "Microscopic Multi-Directional Mechanical Properties of Human Femoral Cancellous Bone Tissue," Key Eng. Mater., **342**, pp. 13–16.

[25] Bryant, J. D., and David, T., 1989, "Rheology of Bovine Marrow," Proc. Inst. Mech. Eng., Part H: J. Eng. Med., **203**(2), pp. 71–75.

[26] Sobotková, E., Hrubá, A., Kiefman, J., and Sobotka, Z., 1988, "Rheological Behaviour of Bone Marrow," Rheol. Acta, **22**, pp. 467–469.

[27] Pan, W., Petersen, E., Cai, N., Ma, G., Lee, J. R., Feng, Z., Liao, K., and Leong, K. W., 2006, "Viscoelastic Properties of Human Mesenchymal Stem Cells," Proceedings of the 27th Annual International Conference on IEEE Engineering in Medicine and Biology Society, Shanghai, China, Vol. 17, pp. 4854–4857.

[28] Thurston, G. B., 1979, "Rheological Parameters for the Viscosity, Viscoelasticity and Thixotropy of Blood," Biorheology, **16**(3), pp. 149–162.

[29] Gefen, A., and Dilmoney, B., 2007, "Mechanics of the Normal Woman's Breast," Technol. Health Care, **15**(4), pp. 259–271.

[30] Vogel, C. R., 2002, *Computational Methods for Inverse Problems*, SIAM, Philadelphia, Chap. 1 and 7.

[31] Hansen, P. C., and O'Leary, D. P., 1993, "The Use of the L-Curve in the Regularization of Discrete Ill-Posed Problems," SIAM J. Sci. Comput. (USA), **14**(6), pp. 1487–1503.